CERN/TC/BEAM 66-4
11.7.1966

ON PROPERTIES OF HYBRID WAVES IN A DISC-LOADED WAVEGUIDE

I.A. Aleksandrov *), V.I. Kotov *) and V.A. Vagin **)

CERN - Geneva

In view of the interest shown recently in such problems, we thought that it would be useful to give a general review of work done on these lines and which has already been published in Russian (1 - 4).

INTRODUCTION

Hybrid waves propagating in a disc-loaded waveguide have several useful and interesting properties, some of which have already found practical applications. For example, the hybrid mode EH_{11}, in special conditions, enables one to obtain a uniform deflecting force over the waveguide aperture, and it is used for the separation of high energy particles.

The question of hybrid waves in such structures has been treated in several papers (5 - 18) from a purely theoretical standpoint, as well as from the point of view of practical applications.

In Refs. 5 and 8 can be found general expressions for the deflecting force, and characteristics of hybrid waves in impedance approximation are considered. A rigorous theory of a deflecting mode is given in Refs. 6, 7, 9, 10. Experimental results on hybrid modes can be found in Refs. 8,11,12,15,18.

In the present paper, we give a consistent, systematic analysis of the dispersion relations of hybrid waves in a lossless disc-loaded waveguide on the basis of small pitch approximation. Such an approximation

*) Institute for High Energy Physics, Serpukhov, USSR.
**) On leave from the High Energy Physics Institute, Serpukhov, USSR.

permits one to find all types of dispersion (anomalous, mixed and positive) and allows the study of propagating, evanescent and complex waves.

On the basis of the above-mentioned approximation, one considers questions related to the choice and optimization of parameters for a disc-loaded waveguide, used as an RF separator deflecting system.

Results are obtained which allow one to choose parameters for the deflecting system, with sufficient practical accuracy.

Our initial data for the choice and the optimization of parameters are compared, whenever possible, with results obtained by other authors on the basis of rigorous theory and experimental results.

I. A GENERAL DISPERSION RELATION FOR PROPAGATING, EVANESCENT AND COMPLEX WAVES IN A DISC-LOADED WAVEGUIDE

In a lossless disc-loaded waveguide, there are hybrid waves corresponding to three types of propagating constants : 1) real (propagating waves), 2) imaginary (evanescent waves), and 3) complex (complex waves). Propagating waves have been investigated in detail for the given structure in Refs. 5,8,16. We shall give below a complete picture of dispersion properties for all given types of hybrid waves, special attention will be given to complex waves.

Complex waves have been studied before in more simple wave-guide structures (e.g., plane with surface impedance[19], magneto-active plasma[20], etc.[21]). In particular, it was shown that they appear in discrete frequency bands. The total flow of energy is always equal to zero for complex waves. Furthermore, such waves can exist in structures where the propagating waves are hybrid.

A detailed study of the dispersion characteristics of complex waves is made more difficult owing to the very complicated mathematical description of their behaviour (especially for closed waveguides). A

detailed study of the properties of complex waves in a simple model coupled to transmission lines has been made in Ref. 22. In Ref. 23 an attempt was made to investigate complex waves in a more complicated structure, namely a cylindrical waveguide with concentric dielectric rod. No dispersion solutions for complex waves were found by these authors[23], but they pointed out some of their regions of existence.

From the point of view of the study of complex waves, the disc-loaded waveguide is the most convenient and practical of all coaxial cylindrical waveguide structures in which the propagating waves have a hybrid character. Certainly, in small pitch approximation it is characterized by only two parameters a/b and d/D (a is the radius of the central hole in the disc, b is the guide radius, D is the pitch, and D is the slot width) and furthermore, the transverse wave number in the disc region is always real. Besides, one finds in a disc-loaded waveguide all kinds of dispersion (anomalous, mixed and positive), which has a strong influence on the diversity of behaviour and properties of complex waves.

In order to obtain a general dispersion relation for all kinds of hybrid waves, let us determine the fields in the central region (region I, $0 \leq r \leq a$) and in the disc region (region II, $a \leq r \leq b$). For the sake of simplicity, let us restrict ourselves to the small pitch approximation ($\lambda >> D$, λ is the wavelength). As usual, let us consider the fields in the form

$$\vec{E}, \vec{H} \sim e^{j(\omega t - \kappa z)} \cdot e^{-i\nu\theta} , \qquad (1)$$

where r, θ, z are the cylindrical co-ordinates, $\kappa = \gamma - j\alpha$ is the complex propagating constant. For convenience, let us split the (t,z) and θ variables by introducing imaginary units j and i in a different form.

Fields are expressed by Herz vectors $\vec{\Pi}_e$ (electric vector) and

by $\vec{\Pi}_h$ (magnetic vector) :

$$\vec{E} = \text{rot rot } \vec{\Pi}_e - jk \text{ rot } \vec{\Pi}_h ,$$

$$Z_o \vec{H} = jk \text{ rot } \vec{\Pi}_e + \text{rot rot } \vec{\Pi}_h , \qquad (2)$$

where $Z_o = 377$ oΩ.

In order to find the fields in the I region, it is convenient to use the transverse vector $\vec{Q}$, introduced by Hahn[6] :

$$\vec{Q} = \left\{ \begin{array}{c} -\frac{j}{k^2} \frac{J_{\nu+1}(k_1 r)}{\gamma_1 J_\nu(k_1 a)} \, i e^{-i\nu\theta} \\ \frac{j}{k^2} \frac{J_{\nu+1}(k_1 r)}{\gamma_1 J_\nu(k_1 a)} \, e^{-i\nu\theta} \\ 0 \end{array} \right\} e^{-j\kappa z} , \qquad (3)$$

where $k_1^2 = k^2 - \kappa^2$ and $\gamma_1 = \frac{k_1}{k}$.

Putting in Eq. (2) $\vec{\Pi}_h = \vec{Q}$ and $\vec{\Pi}_e = i\vec{Q}$, we obtain the following hybrid solutions HM and HE respectively. Fields in region I, omitting the factor exp j ($\omega t - \kappa z$), are represented by a sum of these solutions :

$$E_z = (p + \tfrac{\kappa}{k} q) \frac{J_\nu(k_1 r)}{J_\nu(k_1 a)} e^{-i\nu\theta} , \quad Z_o H_z = -(p\tfrac{\kappa}{k} + q) \frac{J_\nu(k_1 r)}{J_\nu(k_1 a)} \, i e^{-i\nu\theta} ,$$

$$E_r = j \left\{ p\tfrac{\kappa}{k} \frac{J_{\nu+1}(k_1 r)}{\gamma_1 J_\nu(k_1 a)} + q \left[\frac{\kappa^2}{k^2} \frac{J_{\nu+1}(k_1 r)}{\gamma_1 J_\nu(k_1 a)} + \frac{\nu}{kr} \frac{J_\nu(k_1 r)}{J_\nu(k_1 a)} \right] \right\} e^{-i\nu\theta} ,$$

$$E_\theta = j \left\{ p\tfrac{\kappa}{k} \frac{J_{\nu+1}(k_1 r)}{\gamma_1 J_\nu(k_1 a)} + q \left[\frac{J_{\nu+1}(k_1 r)}{\gamma_1 J_\nu(k_1 a)} - \frac{\nu}{kr} \frac{J_\nu(k_1 r)}{J_\nu(k_1 a)} \right] \right\} i e^{-i\nu\theta} , \qquad (4)$$

$$Z_o H_r = -j \left\{ p \left[\frac{\kappa^2}{k^2} \frac{J_{\nu+1}(k_1 r)}{\gamma_1 J_\nu(k_1 a)} + \frac{\nu}{kr} \frac{J_\nu(k_1 r)}{J_\nu(k_1 a)} \right] + q\tfrac{\kappa}{k} \frac{J_{\nu+1}(k_1 r)}{\gamma_1 J_\nu(k_1 a)} \right\} i e^{-i\nu\theta} ,$$

$$Z_o H_\theta = j \left\{ p \left[\frac{J_{\nu+1}(k_1 r)}{\gamma_1 J_\nu(k_1 a)} - \frac{\nu}{kr} \frac{J_\nu(k_1 r)}{J_\nu(k_1 a)} \right] + q\tfrac{\kappa}{k} \frac{J_{\nu+1}(k_1 r)}{\gamma_1 J_\nu(k_1 a)} \right\} e^{-i\nu\theta} ,$$

where p and q are, in general, complex constants.

The representation of fields in Eq. (4) is very convenient. It permits one to obtain immediately, field expressions for the very important special case $\gamma_1 = 0$ ($\beta_\varphi = \frac{v_\varphi}{c} = 1$, where v_φ is the phase velocity, and c is the velocity of light).

We shall take in the II region, the mode $E_{\nu o}$ only. Therefore, we shall put $\vec{\Pi}_h = 0$, for the given region, and choose the Herz **electric** vector $\vec{\Pi}_e$ in its usual form :

$$\vec{\Pi}_e = \left\{ \begin{array}{c} 0 \\ 0 \\ \frac{1}{k^2} \frac{\psi_o(kr)}{\psi_o(ka)} e^{-i\nu\theta} \end{array} \right\} , \tag{5}$$

where

$$\psi_o(kr) = J_\nu(kb)\, N_\nu(kr) - N_\nu(kb)\, J_\nu(kr). \tag{6}$$

In the following, we shall use the function

$$\psi_1(kr) = J_\nu(kb)\, N_{\nu+1}(kr) - N_\nu(kb)\, J_{\nu+1}(kr) , \tag{7}$$

and the following relation exists between ψ_o and ψ_1 :

$$\frac{\partial \psi_o}{\partial(kr)} = \frac{\nu}{kr} \psi_o - \psi_1 . \tag{8}$$

Note that the Herz vector (5) is written taking into account the boundary conditions at $r = b$, and it does not depend on the z co-ordinate. Therefore, fields in region II, taking into account Eqs. (2) and (5), and omitting the time factor $\exp j\omega t$, can be represented in the following form:

$$E_z = A \frac{\psi_o(kr)}{\psi_o(ka)} e^{-i\nu\theta} , \quad Z_o H_r = jA \frac{\nu}{kr} \frac{\psi_o(kr)}{\psi_o(ka)} ie^{-i\nu\theta} ,$$

$$Z_o H_\theta = -jA \left[\frac{\nu}{kr} \frac{\psi_o(kr)}{\psi_o(ka)} - \frac{\psi_1(kr)}{\psi_o(ka)} \right] e^{-i\nu\theta} , \quad H_z = E_\theta = E_r = 0 . \tag{9}$$

Using the boundary conditions at $r = a$, (i.e., $E_z^I = \xi E_z^{II}$, $H_\theta^I = H_\theta^{II}$, $E_\theta^I = E_\theta^{II} = 0$) it is not difficult to find the following system of equations for the complex constants p and q :

$$\begin{cases} p\left[\Psi + \frac{\nu}{ka}(\xi - 1)\right] + q\frac{\kappa}{k}\left(\Psi - \frac{\nu}{ka}\right) = 0 , \\ p\frac{\kappa}{k}\Phi + q\left(\Phi + \frac{\nu}{ka}\right) = 0 , \end{cases} \tag{10}$$

where

$$\Phi = -\frac{J_{\nu+1}(k_1 a)}{\gamma_1 J_\nu(k_1 a)} , \quad \Psi = \frac{\psi_1(kb,ka)}{\psi_o(kb,ka)} + \xi\Phi \quad \text{and} \quad \xi = \frac{d}{D} . \tag{11}$$

Let us introduce the following definition :

$$p = p_1 - jp_2 , \quad q = q_1 - jq_2 , \quad \Phi = \varphi_1 - j\varphi_2 , \tag{12}$$

where p_1, p_2, q_1, q_2, φ_1, φ_2 are real quantities. Putting expressions (12) and $k = \gamma - j\alpha$ into Eq. (10), and equating to zero the imaginary and real parts of each equation, we shall get as a result a system of four linear equations relating the p_1, p_2, q_1, q_2 constants. Then, equating to zero the determinant of this system, we shall find the general dispersion relation for hybrid waves, which, after a series of transformations, takes the following compact form :

$$(M_1 - M_2)^2 + (M_3 - M_4)^2 = 0 , \tag{13}$$

where M_1, M_2, M_3, M_4 are the relative minors of second order :

$$M_1 = \begin{vmatrix} \frac{\gamma}{k}\left(\frac{\psi_1}{\psi_o} + \xi\varphi_1 - \frac{\nu}{ka}\right) + \frac{\alpha}{k}\xi\varphi_2 & -\left(\varphi_1 + \frac{\nu}{ka}\right) \\ \frac{\psi_1}{\psi_o} + \xi\varphi_1 + \frac{\nu}{ka}(\xi - 1) & \frac{\gamma}{k}\left(\frac{\psi_1}{\psi_o} + \xi\varphi_1 - \frac{\nu}{ka}\right) - \frac{\alpha}{k}\xi\varphi_2 \end{vmatrix} ,$$

$$M_2 = \begin{vmatrix} \frac{\gamma}{k}\varphi_2 + \frac{\alpha}{k}\varphi_1 & \varphi_2 \\ -\xi\varphi_2 & -\frac{\gamma}{k}\xi\varphi_2 - \frac{\alpha}{k}\left(\frac{\psi_1}{\psi_o} + \xi\varphi_1 - \frac{\nu}{ka}\right) \end{vmatrix} , \tag{14}$$

$$M_3 = \begin{vmatrix} -\frac{\gamma}{k}\varphi_1 + \frac{\alpha}{k}\varphi_2 & \varphi_2 \\ \frac{\psi_1}{\psi_o} + \xi\varphi_1 + \frac{\nu}{ka}(\xi - 1) & -\frac{\gamma}{k}\xi\varphi_2 - \frac{\alpha}{k}\left(\frac{\psi_1}{\psi_o} + \xi\varphi_1 - \frac{\nu}{ka}\right) \end{vmatrix},$$

$$M_4 = \begin{vmatrix} -\left(\varphi_1 + \frac{\nu}{ka}\right) & \frac{\gamma}{k}\varphi_2 + \frac{\alpha}{k}\varphi_1 \\ \frac{\gamma}{k}\left(\frac{\psi_1}{\psi_o} + \xi\varphi_1 - \frac{\nu}{ka}\right) - \frac{\alpha}{k}\xi\varphi_2 & -\xi\varphi_2 \end{vmatrix}.$$

II. ANALYSIS OF THE GENERAL DISPERSION RELATION AND THE PROPERTIES OF HYBRID WAVES IN DISC-LOADED WAVEGUIDES

In order to obtain a dispersion equation for propagating waves, let us put in Eq. (2) $\frac{\kappa}{k} = \frac{\gamma}{k}$ and $\frac{\alpha}{k} = 0$. Thus, the minors M_2, M_3, M_4 and the φ_2 function, identically become equal to zero, and the dispersion relation (13) takes the well-known form [6,8]:

$$M_1 = 0 ,$$

or

$$\left(1 - \frac{\gamma^2}{k^2}\right)\Psi\Phi + \frac{\nu}{ka}\left[\Psi + \frac{\gamma^2}{k^2}\Phi + \frac{\nu}{ka}(\xi - 1)\right] = 0 . \qquad (15)$$

In an analogous way, putting in relation (13) $\frac{\kappa}{k} = -j\frac{\alpha}{k}$ and $\frac{\gamma}{k} = 0$, we shall get the M_3, M_4 minors and the φ_2 function equal to zero. As a result, the dispersion equation of evanescent waves may be represented by

$$M_1 - M_2 = 0,$$

or

$$\left(1 + \frac{\alpha^2}{k^2}\right)\Psi\Phi + \frac{\nu}{ka}\left[\Psi - \frac{\alpha^2}{k^2}\Phi + \frac{\nu}{ka}(\xi - 1)\right] = 0 . \qquad (16)$$

By comparing Eqs. (15) and (16), it is not difficult to see that they mutually transform into each other, if one replaces $\frac{\gamma}{k}$ by $(-j\frac{\alpha}{k})$, and vice versa.

In order to define the possible regions of existence of complex waves, let us analyse the dispersion properties of propagating waves (Eq. (15)), and of evanescent waves (Eq. (16)).

At cut-off $(\frac{\kappa}{k} = 0)$ these dispersion relations degenerate, and split into two independent and simple equations for cut-off frequencies :

$$\text{a)}\quad J'_\nu(ka) = 0, \qquad \text{b)}\quad J_\nu(kb) + 0.5\pi ka\psi_o(1 - \xi)J'_\nu(ka) = 0 \qquad (17)$$

Let us call $gh_{\nu m}$ -mode the hybrid wave, if its cut-off frequency is equal to $ka = \mu_{\nu m}$, where $\mu_{\nu m}$ is the m^{th} -root of Eq. (17a). Analogously, one introduces $\sigma_{\nu n}$ modes, relative to roots of Eq. (17b). Such a

classification is convenient for further analysis and it has an illusory character in consequence of the peculiarities in the behaviour of dispersion curves of hybrid waves in the neighbourhood of degeneracy of cut-off frequencies for the $gh_{\nu m}$ and $ge_{\nu n}$ modes[1,8,26,27]. The condition for such a degeneracy is known, and it has the form

$$\left(\frac{a}{b}\right)_{\nu mn} = \frac{\mu_{\nu m}}{\sigma_{\nu n}} \quad . \tag{18}$$

The evolution of dispersion curves is shown in Fig. 1, depending on a/b parameters at $\nu = 1$ and $\xi = 1$. One can point out three regions of dispersion of the real branch of the lower mode (upper half-plane), relative to the change of the a/b parameter in the following limits :

1) $0.552 \leqslant \frac{a}{b} \leqslant 1$ - positive dispersion (Fig. 1a,b,c)

2) $0.289 < \frac{a}{b} < 0.552$ - mixed dispersion (Fig. 1d,e,f)

3) $0 < \frac{a}{b} \leqslant 0.289$ - anomalous dispersion (Fig. 1g,h).

At $a/b = 0.480$ the cut-off frequencies of the gh_{11} and ge_{11} modes coincide (see Fig. 1e), whereas for $a/b > 0.480$ of lower modes, the gh_{11} wave appears, and for $a/b < 0.480$, on the contrary, there is the ge_{11} wave.

At $a/b > 0.559$ the evanescent branches of the two lower modes gh_{11} and ge_{11} have a similar character to the corresponding curves of the usual waveguides (lower half-plane, Fig. 1a). At $a/b = 0.559$, the evanescent branches of these waves have a common point of contact A (Fig. 1b) and then ($a/b < 0.559$) these branches are divided into two separate loops 1 and 2, (see, e.g., Fig. 1c). Loop 1 closes the real branches gh_{11} and ge_{11} through the imaginary region at cut-off frequency points. Loop 2 has extremities going to infinity (at $ka \to 0$, $\frac{\alpha}{k} \to \infty$). Between these two loops there is a discrete frequency band. Loop 1 disappears (Fig. 1e) when the cut-off frequencies coincide ($a/b = 0.480$). Subsequently, the given loop 1 appears again on the left of the cut-off frequency of the gh_{11} mode, (see Fig. 1f). On Fig. 1g, together with dispersion curves of the two

lower modes, one shows the curve of the ge_{12} mode. This curve has a very complicated character in the lower half-plane and is divided here into two parts : an undulating branch, going to infinity, and a separate branch 3, which originated when the ge_{12} mode crossed the gh_{12} mode at its cut-off frequency point.

At $a/b = 0.280$ the evanescent branch of the ge_{12} mode has, with loop 1, one common point B (Fig. 1h). At subsequent decreases of the a/b parameter, the mode ge_{12} closes through the imaginary region with gh_{11} (Fig. 1i). More detailed evolutions of dispersion curves of lower hybrid modes, are shown in Figs. 2a,b,c. Dispersion curves for several upper modes (ge_{13}, ge_{14}, ge_{15}, ge_{16} and gh_{12}) are given in Fig. 3 for wider frequency regions at $a/b = 0.3$.

The evanescent branches of these modes have an undulating character and are separated by discrete frequency bands. These bands, as well as the corresponding bands of lower modes, are the regions of existence of complex waves.

In order to obtain dispersion curves of complex waves, it is necessary to solve Eq. (13), which is equivalent to the following system of equations :

$$\begin{cases} M_1 - M_2 = 0 \ , \\ M_3 - M_4 = 0 \ . \end{cases} \qquad (19)$$

Results of this calculation are represented in Fig. 1 by dashed curves. Three forms of the solution of complex waves for lower modes, correspond to three types of dispersions for such modes. (see, e.g., Figs. 1c,f,g).

In the region of positive dispersion, the lower complex mode appears at $a/b < 0.559$, and then the region of existence of this mode becomes wider and the real part of the propagating constant increases, when the a/b parameter decreases. In the region of mixed dispersion ($0.289 < a/b < 0.552$) the real branch of complex waves joins the propagating wave at the point where the group velocity is equal to zero.(see Figs.1e,f,g).

In the region of anomalous dispersion, the real branch of complex waves extends to all regions of phase velocities. (see Figs. 1h,i).

As regards higher complex modes which correspond to two neighbouring propagating waves, then, as is seen from Fig. 3, there is a large collection of them. Each one of these higher complex modes must be characterized by an additional index, which indicates the place of solution in the vertical sections ka = const.

In the next Sections we shall concentrate our attention on practical applications of hybrid waves, for instance, the RF separation of high energy particles. For these purposes, one uses the lower (deflecting) modes with $\nu = 1$, at phase velocity $\beta_\varphi = 1$.

III. THE CHARACTERISTICS OF DEFLECTING MODES AT PHASE VELOCITY EQUAL TO THE VELOCITY OF LIGHT

The dispersion relation (15) for propagating waves at phase velocity $\beta_\varphi = 1$, simplifies considerably :

$$\frac{\psi_1}{\psi_o} - \frac{ka}{\nu+1} = (1 - \xi)\frac{\nu}{ka}\left[1 - \frac{(ka)^2}{\nu(\nu+1)}\right]. \qquad (20)$$

In Fig. 4 are shown curves calculated with the help of Eq. (20) and which determine the conditions of propagation for deflecting modes ($\nu = 1$), at the different values of the ξ parameter. One sees in particular from Fig. 4 and Eq. (20) that in the approximation used by us, the r/b ratio does not depend on the ξ parameter at point $a/\lambda = 0.225$ ($ka = \sqrt{2}$).

One can see in the right bottom corner of Fig. 4 the corresponding curves of the following two hybrid modes with $\nu = 1$ and $\beta_\varphi = 1$.

The field components in the central region, at $\beta_\varphi = 1$, (the

$e^{j(\omega t - \kappa z)}$ factor is omitted) can be represented as (see expressions (4)):

$$E_z = E_o kr \cos\theta , \qquad Z_o H_o = -E_o kr \sin\theta ,$$

$$E_r = E_o\left[\left(\frac{ka}{2}\right)^2 + \left(\frac{kr}{2}\right)^2\right]\cos\theta , \quad Z_o H_r = E_o\left[\left(\frac{ka}{2}\right)^2 - \left(\frac{kr}{2}\right)^2 - 1\right]\sin\theta , \tag{21}$$

$$E_\theta = E_\theta\left[\left(\frac{ka}{2}\right)^2 - \left(\frac{kr}{2}\right)^2\right]\sin\theta , \quad Z_o H_\theta = E_o\left[\left(\frac{ka}{2}\right)^2 + \left(\frac{kr}{2}\right)^2 - 1\right]\cos\theta ,$$

where E_o is the equivalent deflecting field.

The electric field $E = \sqrt{E_r^2 + E_\theta^2 + E_z^2}$ reaches a maximum on the disc radius $(r = a, \theta = 0)$, with respect to expressions (6) :

$$E_{max} = E_o ka \sqrt{1 + \left(\frac{ka}{2}\right)^2} . \tag{22}$$

In order to obtain the power flux P, one integrates the Poynting vector on the waveguide aperture, and for $\beta_\varphi = 1$, one gets

$$P = E_o^2 \frac{\pi a^2}{8 Z_o} (ka)^2 \left[\frac{(ka)^2}{3} - 1\right] . \tag{23}$$

At $ka = \sqrt{3}$ the power flux is equal to zero. In this case the waveguide aperture is split into two regions. In these two regions the partial power fluxes are equal to each other in absolute value, but have opposite signs, (P_+ and P_-).

To determine the boundary between the regions with such partial power fluxes, in an arbitrary case, let us equate to zero the time-averaged Poynting vector :

$$\frac{\left(\frac{ka}{2}\right)^2 - \left(\frac{kr}{2}\right)^2}{\left(\frac{ka}{2}\right)^2 + \left(\frac{kr}{2}\right)^2} \sin^2\theta + \frac{\left(\frac{ka}{2}\right)^2 + \left(\frac{kr}{2}\right)^2 - 1}{\left(\frac{ka}{2}\right)^2 - \left(\frac{kr}{2}\right)^2 - 1} \cos^2\theta = 0 \tag{24}$$

From Eq. (24) it follows that, at $ka = \sqrt{2}$, the boundary between partial power fluxes in opposite directions degenerates and coincides with the disc aperture. For $ka < \sqrt{2}$, Eq. (24) has no solution. This fact and the analysis of the dispersion curves in Fig. 2 allow us to conclude that in the cut-off region $ka < \sqrt{2}$, the positive flux $P_+ = 0$, and there is only a negative power flux P_-. At $ka > \sqrt{2}$ neither partial power flux is equal to zero. In Fig. 5 is shown the division of the waveguide cross-section in the P_+ and P_- regions for $\beta_\varphi = 1$, $\nu = 1$, and at different values of a/λ.

In order to obtain the group velocity, at $\beta_\varphi = 1$, let us differentiate the dispersion equation (15) on κ, and then put $\gamma_1 = 0$. As a result one obtains the following equation for the determination of group velocity :

$$\frac{d\gamma_1^2}{d\kappa}\,\Phi\left(\Psi - \frac{\nu}{ka}\right) + \frac{\nu}{ka}\,\frac{d}{d\kappa}\left[\Psi + \xi\Phi + (\xi - 1)\frac{\nu}{ka}\right] = 0 \,. \qquad (25)$$

At $\beta_\varphi = 1$, one has the following relations :

$$k\,\frac{d\gamma_1^2}{d\kappa} = 2(\beta_g - 1), \quad \frac{k}{\psi_1}\,\frac{d\psi_1}{d\kappa} = \left[\frac{\psi_4}{\psi_1}\,kb + \frac{\psi_o}{\psi_1}\,ka - (\nu + 1)\right]\beta_g \,,$$
$$\frac{k}{\psi_o}\,\frac{d\psi_o}{d\kappa} = \left[\frac{\psi_3}{\psi_o}\,kb - \frac{\psi_1}{\psi_o}\,ka + \nu\right]\beta_g, \quad \frac{k}{\Phi}\,\frac{d\Phi}{d\kappa} = \beta_g + (\beta_g - 1)\frac{(ka)^2}{2(\nu+1)(\nu+2)} \,, \qquad (26)$$

where βg is the group velocity (velocity of light units) and

$$\psi_3 = J'_\nu(kb)\,N_\nu(ka) - N'_\nu(kb)\,J_\nu(ka), \quad \psi_4 = J'_\nu(kb)\,N_{\nu+1}(ka) - N'_\nu(kb)\,J_{\nu+1}(ka) \qquad (27)$$

The functions ψ_0 and ψ_1, ψ_3 and ψ_4 are connected by the relation

$$\psi_4\psi_o - \psi_3\psi_1 = \frac{4}{\pi^2 ka, kb} \,. \qquad (28)$$

Putting Eq. (26) into Eq. (25) and taking into account Eq. (20), after a series of complicated transformations, one gets the following

group velocity equation

$$\beta_g = \frac{A}{A + B} \quad , \tag{29}$$

where $$A = \xi\left[\frac{(ka)^2}{\nu(\nu+2)} - 1\right],$$

$$B = \left[\xi + (1-\xi)\frac{\nu(\nu+1)}{(ka)^2}\right]\cdot\frac{4}{\pi^2(\nu+1)\psi_1^2} - \xi^2\left(\frac{ka}{\nu+1} - \frac{\nu}{ka}\right)(\nu+1) + 2\xi - (\nu+1) + \frac{\nu^2(\nu+1)}{(ka)^2}$$

moreover ka and kb satisfy Eq. (20).

In particular, for $\nu = 1$ and $\xi = 1$, Eq. (29) simplifies considerably :

$$\beta_g = \frac{\frac{(ka)^2}{3} - 1}{1 - \frac{(ka)^2}{6} + \frac{2}{\pi^2\psi_1^2}} \tag{30}$$

Fig. 6 shows as a function of a/λ the group velocity β_g calculated by formula (29) for $\beta_\varphi = 1$, for different values of the parameter ξ (dashed curves).

From Fig. 6, it follows that there are backward waves in the region $0 < a/\lambda < 0.2756$, and that forward waves exist in the region $a/\lambda > 0.2756$. The value $a_o/\lambda = 0.2756$, corresponding to $\beta_g = 0$, does not depend on parameter ξ. As one would expect, the maximal value of the backward group velocity drops when the parameter ξ decreases.

Furthermore, one shows in Fig. 6 the group velocity, calculated by Hahn[7] on the basis of a rigorous theory for different values of the parameter λ/D and for $\xi = 0.8$ (full lines), and the results of experimental calculations of β_g for the deflecting mode, at $\lambda/D = 4,5$ and $\xi = 0.8$. A comparison of all these data shows that when the λ/D parameter increases, for fixed values of ξ, the group velocity crosses the frequency axis more to the right, and the maximal value of the backward group velocity grows.

Thus for instance for the cases $\lambda/D \to \infty$, (small pitch approximation) and $\lambda/D = 4$, the values of the frequency where the group velocity crosses the axis, are given, are given, respectively, by $(a_o/\lambda) = 0.2756$ and $(a_o/\lambda) = 0.2505$, i.e., they differ by 10%. In the region in which we are interested, $-0.04 < \beta_g < +0.05$, such a relative difference in frequencies of these curves is approximately conserved.

The existence of regions of forward and backward waves for a deflecting mode permits one to choose (in contrast to circularly symmetrical E waves), if necessary, a group velocity as small as is wanted and of either sign, while obtaining at the same time a finite aperture $2a/\lambda$. However, it may be shown that when the group velocity decreases, the requirements for the accuracy of fabrication and the maintenance of the geometrical parameters of the waveguide and the frequency stability sharply increase.

Thus, the deviation of the phase velocity from the velocity of light, due to the errors of the waveguide size and frequency, may be represented by

$$\Delta\beta_\varphi = \frac{\partial\beta_\varphi}{\partial\lambda}\left[\Delta\lambda + \sum_i \rho_i \, \Delta q_i\right], \tag{31}$$

where ρ_i is the relative "weight" corresponding to the geometrical parameter q_i. The derivative $\frac{\partial\beta_\varphi}{\partial\lambda}$ at $\beta_\varphi = 1$, increases as $1/\beta_g$ when the group velocity decreases

$$\frac{\partial\beta_\varphi}{\partial\lambda} = \frac{1}{\lambda}\left(\frac{1}{\beta_g} - 1\right) . \tag{32}$$

The relative requirements for the waveguide parameters may be found by comparing the weighting function

$$\rho_i = \frac{\partial\beta_\varphi}{\partial q_i} \Big/ \frac{\partial\beta_\varphi}{\partial\lambda} . \tag{33}$$

The weighting functions can be obtained in a similar manner to the group velocity (see Eqs. (25), (26) and (27)).

For example, for $\nu = 1$, $\xi = 1$, and for a and b parameters the weighting functions are :

$$\rho_a = \frac{\left(\frac{ka}{2}\right)^2 - 1}{\left[\frac{(ka)^2}{3} - 1\right]\left(\frac{1}{\beta_g} - 1\right)^{a/\lambda}} \qquad (34)$$

and

$$\rho_b = \frac{1 - \frac{(ka)^2}{6} - \frac{\frac{(ka)^2}{3} - 1}{\beta_g}}{\left[\frac{(ka)^2}{3} - 1\right]\left(\frac{1}{\beta_g} - 1\right)^{b/\lambda}} , \qquad (35)$$

where a/λ and b/λ are related by Eq. (15). On Fig. 7 one gives these functions in relation to a/λ.

The functions ρ_d and ρ_D may be obtained only with the help of a rigorous theory.

Deflecting forces on a traversing particle with charge e can be expressed only by longitudinal field components[5]

$$\vec{F} = \frac{e}{\kappa}\left\{\frac{1 - \beta_\varphi \beta}{1 - \beta_\varphi^2} \nabla_\perp E_z + \frac{\beta - \beta_\varphi}{1 - \beta_\varphi^2}\left[\vec{i}_z \nabla_\perp H_z\right]\right\} e^{j\left[\omega t\left(1 - \frac{\beta}{\beta_\varphi}\right) + \tau_o\right]} , \qquad (36)$$

where $\nabla_\perp = \vec{i}_r \frac{\partial}{\partial r} + \vec{i}_\theta \frac{1}{r}\frac{\partial}{\partial \theta}$; $\vec{i}_r$, $\vec{i}_\theta$, $\vec{i}_z$ are the unit vectors ; β is the velocity of particles in units of the velocity of light, and τ_o is the initial phase of flight.

In the case when $\beta_\varphi = \beta = 1$, Eq. (36) simplifies considerably and the maximal value of the force is represented as follows :

$$\vec{F}_{\perp m} = \frac{e}{k} \nabla_\perp E_z \qquad (37)$$

Introducing into Eq. (27) the component E_z from Eq. (21), we get, at $\nu = 1$:

$$\vec{F}_{\perp m} = e E_o (\vec{i}_r \cos\theta - \vec{i}_\theta \sin\theta) . \qquad (38)$$

One sees from the above that the deflecting force, at $\beta_\varphi = \beta = 1$ is constant over the whole aperture, and E_o is the equivalent deflecting field at the feed point.

Let us give an estimate of the non-uniformity of the force over the aperture in the case of a shift of the phase velocity from the velocity of light ($|\beta_\varphi - 1| \ll 1$, $B = 1$). For this one uses formulae (36) and (37), Eqs. (15) and (20), and expressions of the field components E_z and H_z(4) for an arbitrary phase velocity. Taking into account the condition $|\beta_\varphi - 1| \ll 1$, after tedious calculations, one gets the following simple expression

$$\frac{E_o(\beta_\varphi,0) - E_o(\beta_\varphi,r)}{E_o(\beta_\varphi,0)} = -\frac{1}{2}(\beta_\varphi - 1)(kr)^2 . \qquad (39)$$

From the point of view of the characteristics of a practical deflecting waveguide, a convenient parameter is the equivalent strength of electric field normalized to power

$$\eta = \frac{E_o \lambda}{\sqrt{P}} . \qquad (40)$$

In small pitch approximation, using the equation of power flux (23), we get the following expression :

$$\eta = \frac{4}{(ka)^2}\sqrt{\frac{6\pi Z_o}{(ka)^2 - 3}} . \qquad (41)$$

In Fig. 8, are shown graphs of η for two values of the parameter $\xi = 0.8$ and 1.0, as well as the relation E_o/E_{max} (dashed line) as functions of group velocity. In this figure are also given the points of

equivalent, normalized values of the field. They are obtained by a rigorous theory for $\lambda/D = 4$ and $\xi = 0.8$.[7]

A slight difference between the values obtained on the basis of a rigorous theory and small pitch approximation respectively is observed only in the region of very low group velocities, ($|\beta_g| < 0.005$) in the interval under consideration, i.e., $-0.04 < \beta_g < +0.05$.

IV. OPTIMUM PARAMETERS OF A DEFLECTING WAVEGUIDE *)

Keeping in the limits of small pitch approximation, we shall consider the problem of the optimization of a deflecting RF separator system.

A deflector imparts to an ultrarelativistic particle having longitudinal momentum p_o, a transverse angle :

$$\epsilon = \frac{p_\perp}{p_o} , \tag{42}$$

where $p_\perp$ is the transverse momentum.

For an RF separator with two deflectors the required deflection is found from a well-known condition of the optimum utilization of the vertical acceptance[28]

$$\begin{cases} \epsilon = \epsilon_o , & (43a) \\ p_\perp = \frac{\sqrt{2}}{6} \frac{a/\lambda}{\ell} p_o , & (43b) \end{cases}$$

where $2\epsilon_o$ is the initial angular divergence of particles in the

*) The problem of the optimization of deflector design has been also treated by Hahn and Halama, in a very interesting paper[18].

vertical plane at input to the first deflector, $\bar{\ell} = \ell/\lambda$, ℓ is the length of deflector.

Using the expressions for a deflecting force (38), and taking into account the attenuation in amplitude of the wave in the waveguide, we find, for a transverse momentum :

$$p_\perp c = e E_o \frac{1 - e^{-\delta\ell}}{\delta\ell} , \qquad (44)$$

where $\delta\ell = \frac{\pi\bar{\ell}}{Q\beta_g}$, and Q is the quality factor of the waveguide.

For the following, it is convenient to introduce a normalized transverse momentum :

$$\frac{p_\perp c}{\sqrt{P}} = \frac{10^{-3}}{\pi} c\,\eta\,Q\,\beta_g (1 - e^{-\delta\ell}) \left[\frac{\text{MeV}}{\sqrt{\text{MW}}}\right] , \qquad (45)$$

where the value $e\eta$ is taken in $(\text{keV}/\sqrt{\text{MW}})$ units.

In Fig. 9 is shown the normalized momentum $\frac{p_\perp c}{\sqrt{P}}$ as a function of group velocity, calculated with Eq. (45), taking into account Eqs. (20), (29) and (41), for different values of $\bar{\ell}$ and $\xi = 0.8$. The quality factor Q is fixed and equal to 10^4, which is close to the value obtained in practice for S band (10 cm wavelength).

As is evident from Fig. 9, in the region of very low group velocities, the efficiency of the deflection drops sharply. This is explained by the fact that - in spite of the increase of the normalized field strength η as $\beta_g \to 0$ - the factor due to the attenuation of the wave appears to be more important. On both sides of the value $\beta_g = 0$, there are maxima which, when $\bar{\ell}$ increases, are displaced from the ordinate axis (in particular, for small $\bar{\ell}$, for example $\bar{\ell} = 10$, the maxima are so close to the ordinate axis that they could not be shown on the chosen scale).

In Fig. 9 are also given the corresponding points for $\lambda/D = 4$, $\xi = 0.8$ and $Q = 10^4$, calculated by a rigorous theory. A comparison of the results shows that in the considered range of β_g there is good agreement between approximate curves and exact data, everywhere except in the region of very small group velocities, ($|\beta_g| < 5.10^{-3}$).

The presence of maxima for curves with transverse momentum determines, for the fixed power and length of the guide, two optimum values for group velocity (smaller than and greater than zero). Which of these optimum values should be preferred may be decided upon after a more refined analysis of various additional factors, related to the total acceptance and the transverse momenta, to the presence or absence of spurious modes which are due to the turning over of the dispersion curve. However, such an approach does not give the possibility of solving the problem of the effective utilization of the deflectors.

Unlike linear accelerators, in deflecting RF separator systems it is necessary to provide operating conditions on a limiting breakdown level. Only then will it be possible to obtain maximum acceptance for the deflector, and consequently a sufficient intensity of separated particles in a region of the energetic spectrum with maximum momentum of secondaries.

Consideration of the limiting electrical strength in deflectors is a very difficult problem, and it depends to a considerable degree on the technology of fabrication, on the conditions of the surfaces, on vacuum system cleanliness, and on the geometrical configuration of the waveguide.

Experimental values of the limiting field strength E_{max} for disc-loaded waveguides at S band, are around 200 kV/cm[24]. Using this value, let us determine the limiting power P_{max}, and the limiting transverse momentum $(p_\perp c)_{max}$ expressing the power flux by E_{max}, in accordance with Eqs. (22) and (23)

$$P = \frac{(E_{max}\lambda)^2}{24\pi Z_0} \frac{(ka)^2[(ka)^2 - 3]}{(ka)^2 + 4} . \qquad (46)$$

Putting in Eq. (46) the limiting value $E_{max}\lambda = 2$ Mv and considering in Eqs. (25), (45) and (46), the frequency term ka as an intermediate variable, we shall find P_{max} and $(p_\perp c)_{max}$ as functions of the group velocity (see Fig. 10). In the considered region of values of β_g, the limiting power P_{max} varies practically linearly with the group velocity (dashed lines).

For comparison, in the region $\beta_g < 0$ of Fig. 10 is plotted also a field strength value (black triangle) which could be applied in the deflecting waveguide od the Brookhaven RF separator[25].

Graphs for the limiting transverse momentum (full lines) differ essentially from the corresponding curves $p_\perp c / \sqrt{P}$, which are given in Fig. 9. The region of low group velocities, where the values $(p_\perp c)_{max}$ decrease, is considerably larger in Fig. 10. For $\beta_g > 0$ and for different fixed values of $\bar{l}$, the limiting transverse momentum has a flat maximum. In Fig. 10 is shown also the function $(\frac{a}{a_o})^4$, (curve I), where a_o is the radius of the discs at $\beta_g = 0$. This value, for a fixed waveguide length, is proportional to the total acceptance of the deflector

$$R = \frac{1}{3} (\frac{a_o}{\lambda})^4 (\frac{a}{a_o})^4 \frac{\lambda^2}{\bar{l}^2} \quad . \tag{47}$$

The circles represent the values of $(a/a_o)^4$ obtained on the basis of a rigorous theory for $\lambda/D = 4$ and $\xi = 0.8$. In the region $-0.02 < \beta_g < 0.06$ one observes a good agreement between the results of small pitch approximation and those of the rigorous theory. In this range of group velocity, the function $(a/a_o)^4$ is represented, to a very high degree of accuracy, by the linear function

$$(\frac{a}{a_o})^4 = 11 \beta_g + 1 \tag{48}$$

Using the results shown in Fig. 10, one can give a univalued choice of optimal parameters for the deflecting waveguide.

Let us examine, as an example, the region $\beta_g > 0$. The existence of flat maxima on the curves $(p_\perp c)_{max}$ for given $\bar{\ell}$, provides a relatively free choice of group velocity. However, efforts to reduce the level of power (dashed line on Fig. 8) make it necessary to decrease the group velocities. As a compromise, one can choose values of $(p_\perp c)_{max}$, for instance, at the level 0.95 from the maxima of the corresponding curves, towards low group velocities. From this one determines the set of parameters $(p_\perp c, P, \bar{\ell}, \beta_g)$. With Eqs. (29) and (43), one can find the dependence of this set of optimum parameters on the longitudinal momentum (see Fig. 11).

Let us compare the regions $\beta_g > 0$ and $\beta_g < 0$; for instance for $\beta_g > 0$ and a longitudinal momentum $p_o = 10$ GeV/c one gets as parameters $\beta_g = 0.0195$, $P_{max} = 20.5$ MW, $(p_\perp c)_{max} = 20.4$ MeV, and $\bar{\ell} = 31.7$ (see Fig. 11). For these same values of the transverse momentum and level of power in the region $\beta_g < 0$, the corresponding parameters are : $\beta_g = -0.0195$, $\bar{\ell} = 25.5$ and $R_- = 0.95\ R_+$.

From the point of view of full acceptance, a similar situation holds quite closely, as well as for larger values of the longitudinal momentum. From this follows a practical equivalence of the regions $\beta_g > 0$ and $\beta_g < 0$. The given scheme for choosing parameters for a deflecting waveguide is exhaustive; in particular in the small pitch approximation, the question of the choice of the parameter λ/D, cannot be solved. An exact theory allows one in principle, to obtain an optimum value of this parameter. An exact theory can also introduce some corrections of the values of the sets of optimum parameters obtained. However, if one takes into account the indefinite nature of the breakdown field value, then one can consider that the accuracy provided by small pitch approximation is quite satisfactory.

One can extend the results obtained to other frequency bands. For this it is necessary to express the values E_{max} and Q as functions of the wavelength ($E_{max} \sim \frac{1}{\sqrt{\lambda}}$ and $Q \sim \sqrt{\lambda}$) in expressions (43), (45)

and (46), and to introduce the following generalized parameters $\frac{\ell}{\lambda\sqrt{\lambda}}$, $\frac{P}{\lambda}$, $\frac{p_\perp c}{\lambda}$, $\frac{p_o c}{\lambda\sqrt{\lambda}}$ u β_r.

It is also not difficult to show than, starting with a definite value of the longitudinal momentum, it is more advantageous (from the point of view of full acceptance, power, and practical performance) not to allow unrestricted increase of group velocity, but to use a deflector composed of several shorter sections with separate feed.

CONCLUDING REMARKS

In Section IV, we have only outlined a scheme for the choice of parameters of a deflecting waveguide, without claiming in any way that it is a universal one.

A series of practical factors (such as: power of RF tubes, cost. ratio between full acceptance of deflectors and beam optics, intensity of secondaries, etc.) degree can have an influence, to a certain extent, on this choice.

The above-mentioned optimization scheme appears as a consistent and extreme case of the full utilization of the total acceptance of a deflecting waveguide.

One of the authors (V.A.V.) wishes to thank Dr. P. Bernard and Dr. H. Lengeler for many useful discussions. He is grateful to Professor Ch. Peyrou for the hospitality extended to him at CERN, and Mrs. M. Bell for a careful reading of the manuscript.

FIGURE CAPTIONS

Fig. 1. Evaluation of dispersion curves for $\nu = 1$ and for different values of the parameters a/b. (The solutions for complex waves are presented by dashed lines).

Fig. 2. Dispersion curves of lower hybrid modes at $\nu = 1$.

Fig. 3. Dispersion curves for higher hybrid, complex and evanescent waves.(The solutions for complex waves are given for only one frequency band by dashed lines).

Fig. 4. Condition of propagating hybrid waves at $\nu = 1$, and $\beta_\varphi = 1$.

Fig. 5. The regions of positive (internal) and negative (external) power fluxes for different values of a/λ.

Fig. 6. Group velocity as function of a/λ at $\beta_\varphi = 1$.

Fig. 7. Weighting functions of parameters a and b, depending on a/λ.

Fig. 8. Normalized equivalent field strength (full lines) and the relation E_o / E_{max} (dashed lines) as functions of group velocity.

Fig. 9. Normalized transverse momentum as a dunction of group velocity (parameter a/λ).

Fig. 10. Limiting power (dashed lines) and limiting transverse momentum (full lines) as functions of group velocity. (Curve I represents the relation $(a/a_o)^4$).

Fig. 11. Optimum parameters of the deflecting waveguide, as functions of the longitudinal momentum in the region $\beta_g > 0$.

REFERENCES

1. V.A. Vagin, V.I. Kotov and M.M. Ophizerov, Dubna preprint P-2274 (1965).
2. I.A. Aleksandrov, V.A. Vagin and V.I. Kotov, Dubna preprint P-2503 (1965).
3. I.A. Aleksandrov, V.A. Vagin and V.I. Kotov, Dubna preprint P-2507 (1965).
4. V.A.Vagin and V.I. Kotov, Soviet Tech. Phys. 36, 453 (1966).
5. Y. Garault, Compt.rend. 254, 843 (1962); 254, 1391 (1962); 255, 2920 (1962).
6. H. Hahn, Rev. Sci. Instr. 34, 1094 (1963).
7. H. Hahn, Brookhaven preprint BNL AADD-54 (1964).
8. Y. Garault, CERN report 64-43 (1964).
9. H.G. Hereward and M. Bell, CERN report 63-33 (1963).
10. H.G. Hereward and M. Bell, CERN report 65-37 (1965).
11. O.H. Altenmueller, R.R. Larsen and G.A. Loew, Rev. Sci. Instr. 35, 438 (1964).
12. P. Bramham, CERN internal report AR/Int.P Sep/63-4 (1963).
13. M. Bell, P. Bramham and B.W. Montague, Nature 198, 277 (1963).
14. M. Bell, P. Bramham, R.D. Fortune, E. Keil and B.W. Montague, Proc. Int.Conf. on High Energy Accelerators, Dubna (1963), (Atomizdat, Moscow, 1964, p. 798).
15. R. Hirel, Nucl. Instr. Methods 26, 90 (1964).
16. V.A. Vagin, CERN preprint TC/BEAM 66-3 (1966).
17. H. Lengeler, CERN preprint TC/BEAM 65-4 (1965).
18. H. Hahn and H.I. Halama, Rev. Sci. Instr. 36, 1788 (1965).
19. M.A. Miller, Doklady Acad. Nauk SSSR 85, 571 (1952).
20. B.N. Gershman, Pamiati Andronova, Ed. Acad. Nauk SSSR, 599 (1959).
21. V.I. Talanov, Radiophysica 3, 802 (1960).
22. A.M. Boljanzev and A.V. Gaponov, Radiotech. and Electr. 9, 1188 (1964).
23. P.I. Clarricoats and B.C. Taylor, Proc. IEE 111, 1951, (1964).
24. R.P. Borghi, Al.L. Eldredge, G.A. Loew and R.B. Neal, Stanford preprint SLAC-PUB-71 (1965).
25. H. Hahn, H.I. Halama and H.W. Foelshe, Int. Conf. on High Energy Accelerators, Frascati (1965), to be published.
26. P.I. Clarricoats, Proc. IEE 110, 261 (1963).
27. R.A. Waldron, Proc. IEE 111, 1659 (1964).
28. W. Schnell, CERN report 61-5 (1961).

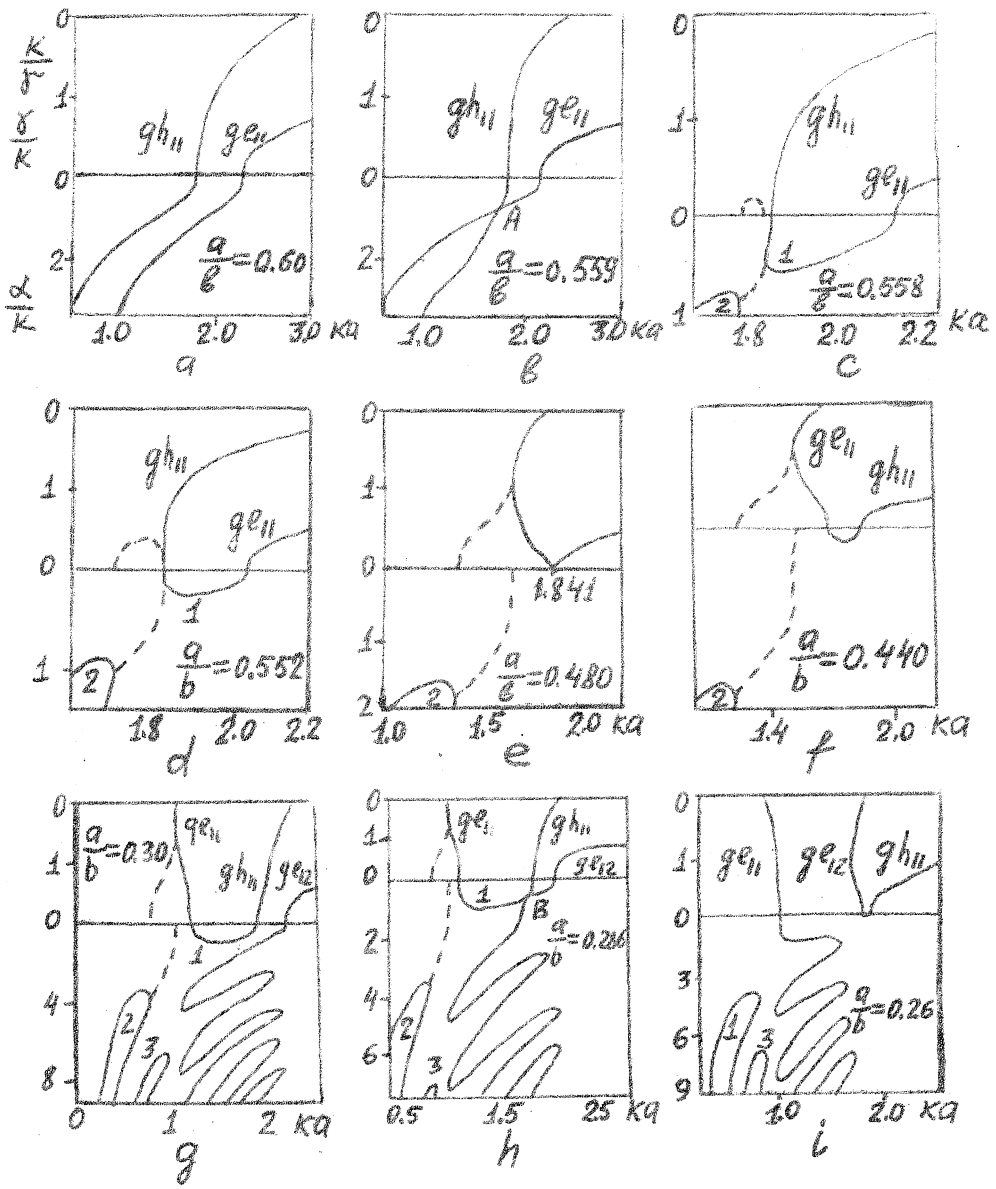

Fig. 1

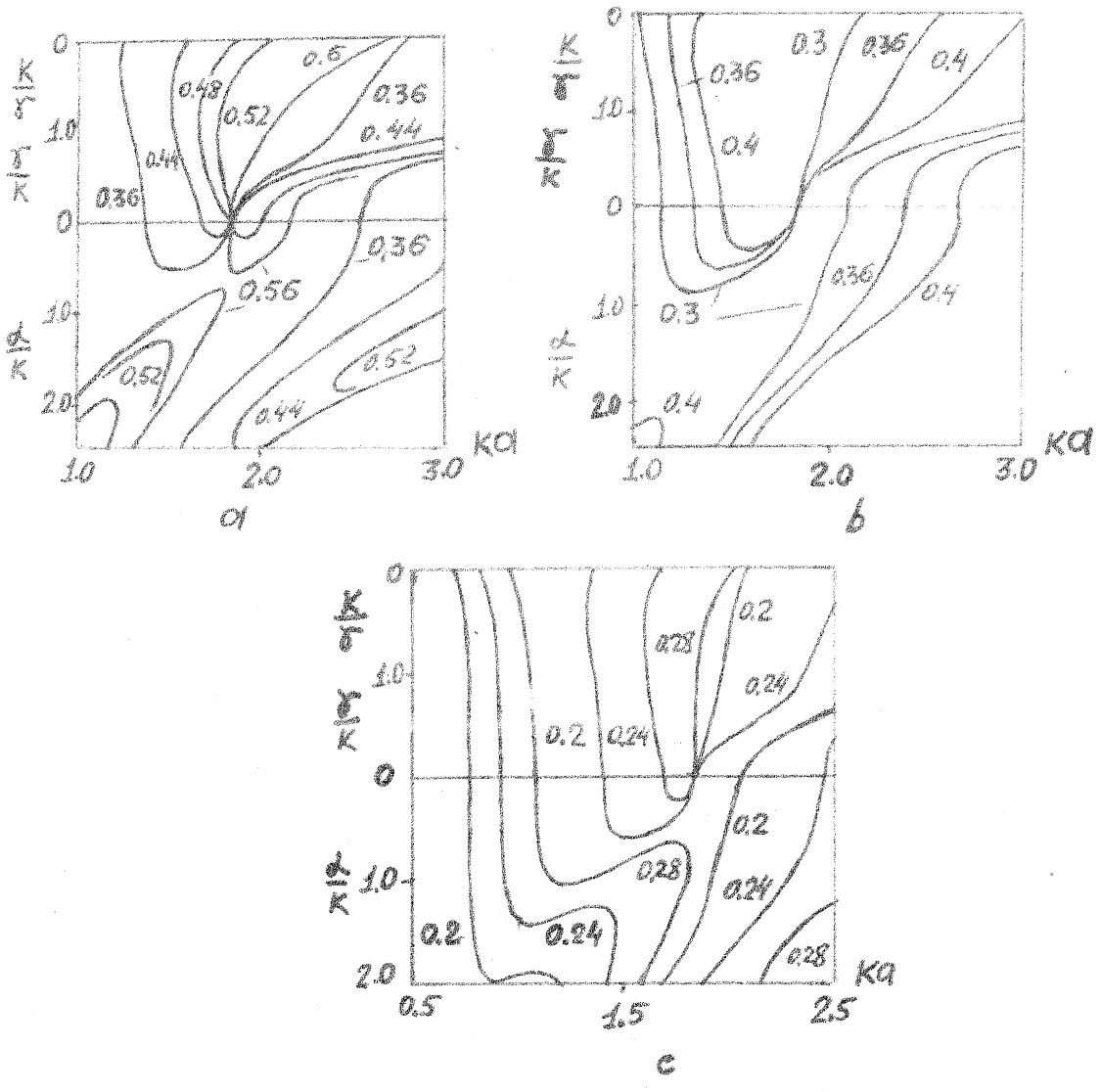
K/γ
δ/K
d/K
0
1.0
2.0
0.36
0.44
0.48
0.52
0.56
0.6
1.0
2.0
3.0
ka
a
0.3
0.4
b
0.2
0.24
0.28
0.5
1.5
2.5
c

Fig. 2

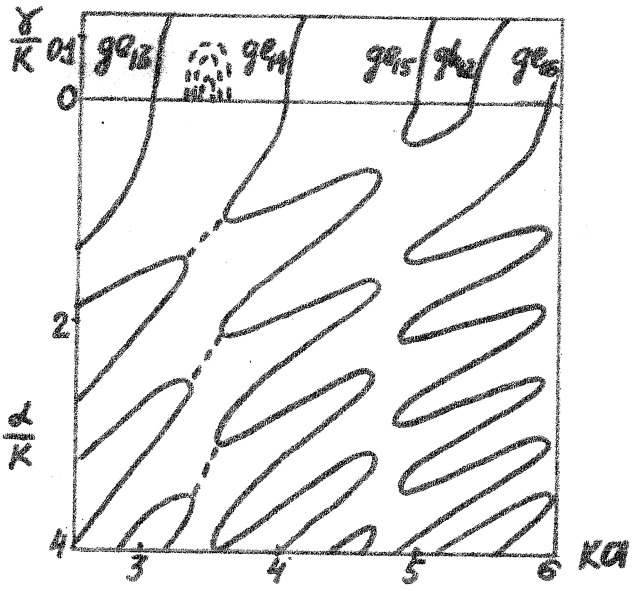

Fig. 3.

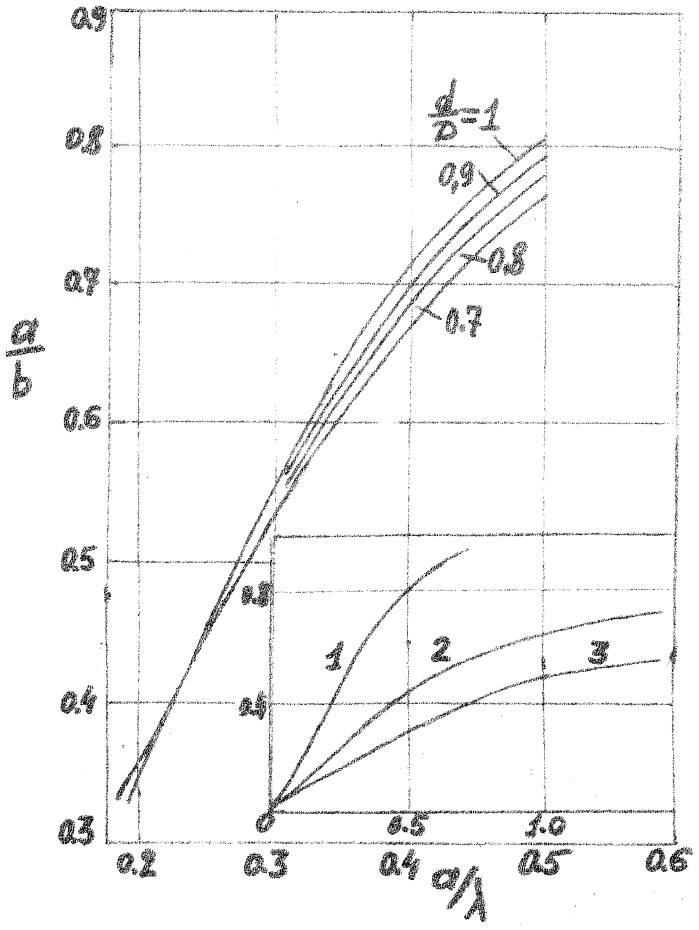

Fig. 4.

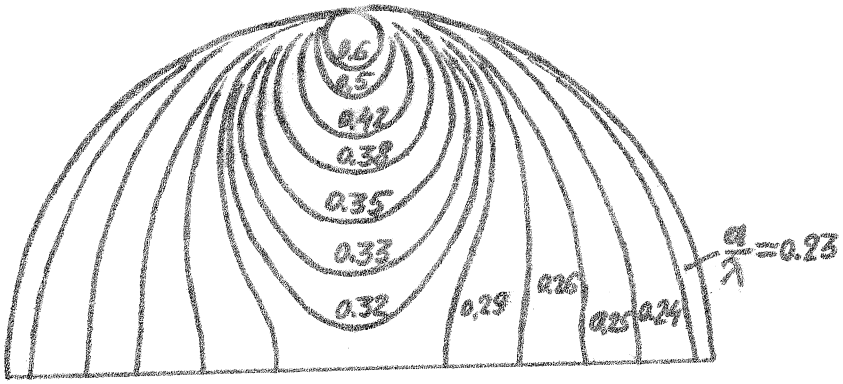
0.42
0.38
0.35
0.33
0.32
0.29
0.26
0.25
0.24
$\frac{a}{\lambda}=0.23$

Fig. 5.

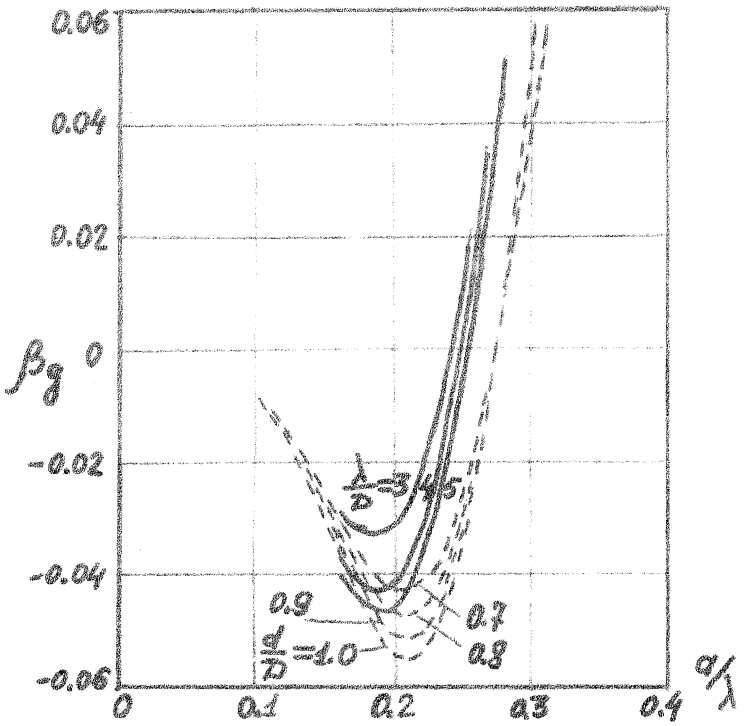
0.06
0.04
0.02
β_g 0
-0.02
-0.04
-0.06
0
0.1
0.2
0.3
0.4
$\frac{a}{\lambda}$
$\frac{\lambda}{D}=3$
0.9
0.7
$\frac{d}{D}=1.0$
0.8

Fig. 6.

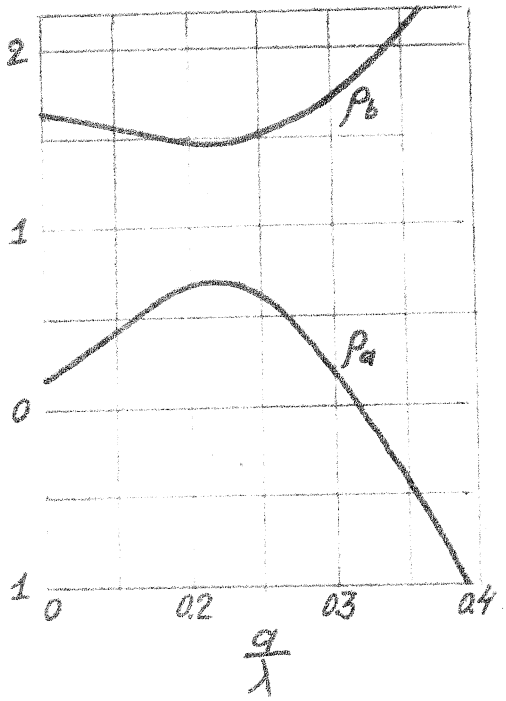
2
1
0
1
ρ_b
ρ_a
0
0.2
0.3
0.4
$\frac{a}{\lambda}$

Fig. 7

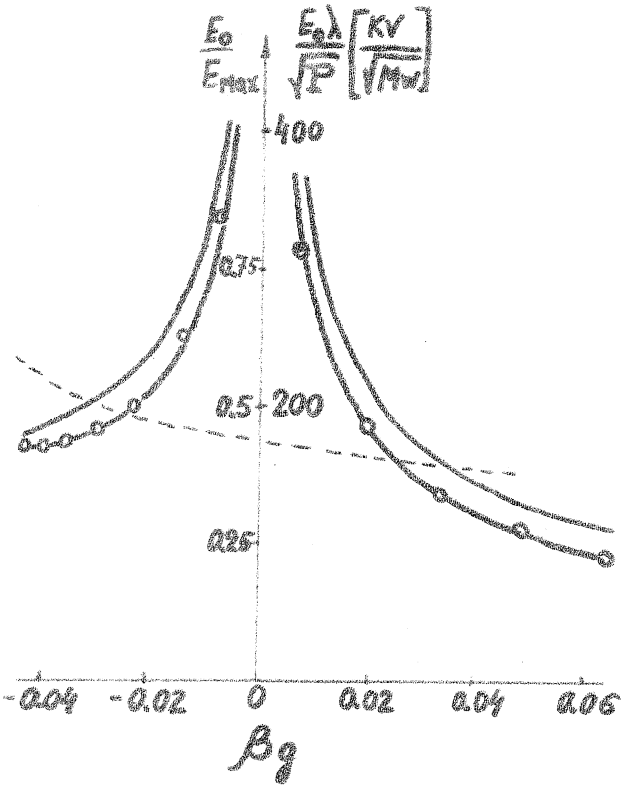
$\frac{E_0}{E_{max}}$
$\frac{E_0 \lambda}{\sqrt{P}} \left[\frac{KV}{\sqrt{MW}}\right]$
400
0.75
0.5
200
0.25
-0.04
-0.02
0
0.02
0.04
0.06
β_g

Fig. 8

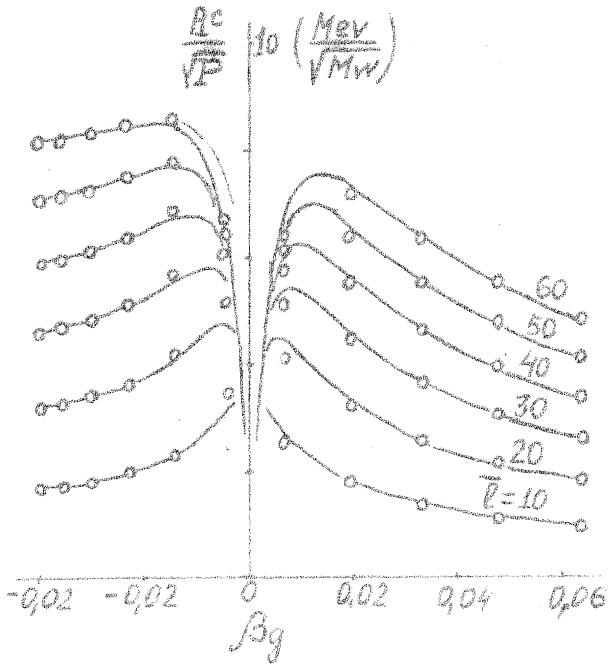
$\frac{Rc}{\sqrt{P}}$
10 $\left(\frac{Mev}{\sqrt{Mw}}\right)$
60
50
40
30
20
$\ell = 10$
-0,02
-0,02
0
0,02
0,04
0,06
βg

Fig. 9.

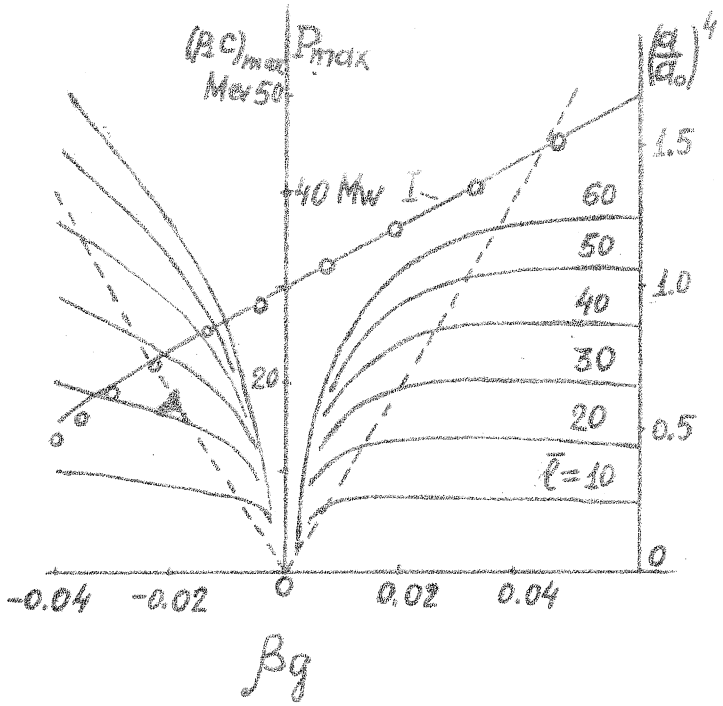
$(Rc)_{max}$
Mev 50
P_{max}
40 Mw
60
50
40
30
20
$\ell = 10$
20
$\left(\frac{a}{a_0}\right)^4$
1.5
1.0
0.5
0
-0.04
-0.02
0
0.02
0.04
βg

Fig. 10.

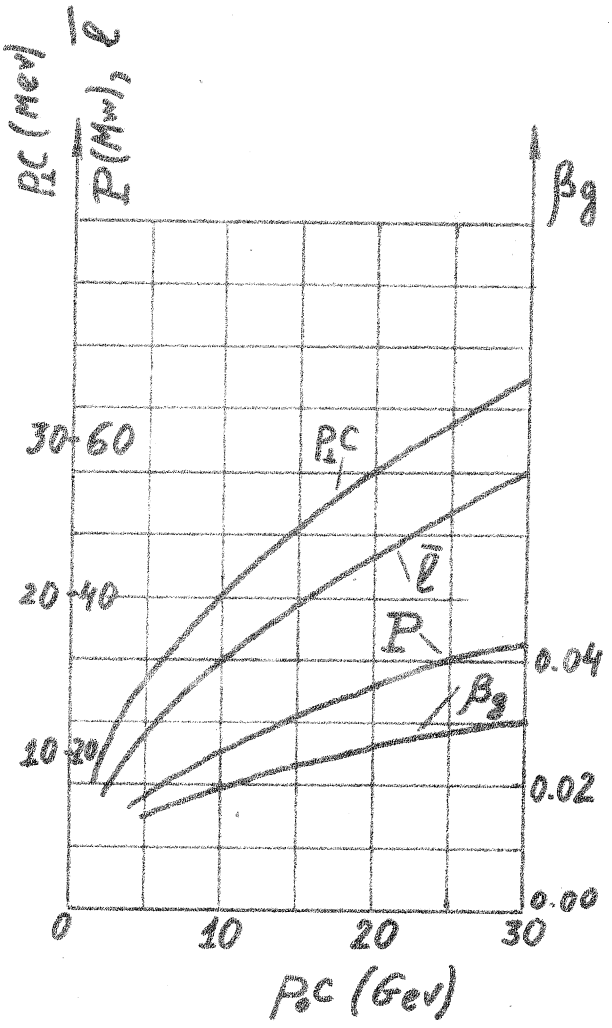
Pc (Mev)
R (M)
β_g
30-60
20-40
10-20
P_c
$\bar{\ell}$
R
β_g
0.04
0.02
0.00
0
10
20
30
Pc (Gev)

Fig. 11.